Experimental validation and numerical analyses of a new steel post-tensioned connection for high-seismic- performance moment-resisting frames

Vasdravellis, George; Karavasilis, Theodore; Uy, Brian

Publication date:
2012

Experimental validation and numerical analyses of a new steel post-tensioned connection for high-seismic-performance moment-resisting frames

G. Vasdravellis & B. Uy
Institute for Infrastructure Engineering, University of Western Sydney, Australia

T.L. Karavasilis
School of Engineering, University of Warwick, UK

SUMMARY:
Self-centering steel moment resisting frames have been developed as an alternative to conventional steel moment resisting frames aiming to eliminate structural damage and to minimize residual drifts under the design earthquake. In the present work, a new typology for self-centering beam-to-column connections is proposed and validated experimentally and numerically. The connection makes use of post-tensioned high-strength strands which provide the required strength and self-centering capacity. A new energy-dissipation system (ED) which can be easily replaced after the design earthquake is introduced. The connection performance is experimentally validated under quasi-static cyclic loading conditions. The experimental results show that the proposed connection exhibits robust self-centering behaviour up to 6% interstory drifts and adequate energy dissipation capacity. Nonlinear finite element models are constructed to capture the cyclic behaviour of the connection. The numerical models are then used to assess the connection performance and all possible failure modes.

Keywords: post-tensioning; self-centering; steel moment-resisting frames; energy-dissipation.

1. INTRODUCTION

Conventional ductile steel moment-resisting frames (MRFs) are currently designed to form a global plastic mechanism under strong earthquakes through the development of plastic hinges at the end of beams and at the base of the columns (Eurocode 8, 2004). This design approach provides well known advantages such as acceptable behavior able to protect human life, economy, low base shear force and controlled total floor accelerations. However, plastic hinges in structural members involve significant cyclic inelastic deformations and local buckling which result in difficult to inspect and repair damage as well as residual drifts. Therefore, conventional steel MRFs result in socio-economical losses such as damage repair costs and loss of building use or occupation after a major seismic event. In addition, they may result in building demolition due to the complications associated with repairing large residual drifts. Research efforts developed self-centering steel moment resisting frames (SC-MRFs) with post-tensioned (PT) connections (e.g. Garlock et al., 2002, Christopoulos et al., 2002, Chou at al., 2006). SC-MRFs have the potential to eliminate inelastic deformations and residual drifts under strong earthquakes as the result of several features: softening force-drift behavior due to separations (gap openings) developed in beam-to-column connections; re-centering capability due to elastic pre-tensioning elements (e.g., high strength steel bars) providing clamping forces to connect beam and columns; and energy dissipation capacity due to energy dissipation elements (EDs) which are activated when gaps open. When properly designed, these EDs can be easily inspected and replaced. In this paper, a new SC beam-to-column connection typology is proposed. The connection uses PT high-strength steel bars to provide self-centering capability and new EDs consisting of yielding web hourglass pins (WHPs) which can be very easily replaced if damaged. The connection performance is experimentally validated under quasi-static cyclic loading conditions. The experimental results show that the proposed connection exhibits robust self-centering behavior up to 6% interstory drifts and adequate energy dissipation capacity. The connection specimens are imposed to drift levels far beyond the expected design ones to identify all possible failure modes. Nonlinear finite element models

(FEM) were employed to further assess the connection performance and to study how various parameters influence the cyclic performance and the ultimate failure modes of the proposed typology.

2. STEEL POST-TENSIONED CONNECTION WITH WEB HOURGLASS PINS

Fig. 1(a) shows the PT connection proposed by the authors (Vasdravellis et al., 2012). Two high strength steel bars located at the mid-depth of the beam, one at each side of the web, pass through holes drilled on the column flanges. The bars are post-tensioned and anchored to the exterior column flange, and horizontally clamp the beam to the column. Four cylindrical steel pins (WHPs) are inserted in aligned holes drilled on the web of the beam and on strong supporting plates. The supporting plates are welded to the column flanges and have large thickness to provide fixed support boundary conditions to WHPs. Energy dissipation is provided by inelastic bending of the WHPs which are symmetrically placed (close to the top and bottom beam flange) to provide increased lever arm and increased internal moment resistance. As shown in Fig. 1(b), WHPs are designed to have an optimized hourglass shape to provide enhanced energy dissipation and fracture capacity (Kobori et al., 1992). Both sides of the beam web are reinforced with steel plates to increase the contact surface of the WHPs with the web. In that way, possible ovalization of the holes drilled on the web under the WHP bearing forces becomes negligible and pinching behavior under cyclic deformations can be avoided. The connection includes beam flange reinforcing plates to avoid excessive early yielding in the beam flanges under the high PT bars forces. In addition, the panel zone is strengthened with horizontal stiffeners and continuity plates along the web of the column.

Two connection specimens, SC-WHP1 and SC-WHP2, were tested by the authors under quasi-static cyclic loading conditions in the test setup shown in Fig. 1(c) (Vasdravellis et al., 2012). Specimen SC-WHP1 (Fig. 2(a)) was designed according to the procedure proposed by Garlock et al. (2007). Specimen SC-WHP2 (Fig. 2(b)) was identical to SC-WHP1 apart from additional reinforcing details in the beam according to Kim and Christopoulos (2009), i.e., welded longitudinal stiffeners on the web of the beam and four 27mm-diameter holes drilled on the beam flanges immediately after the end of the reinforcing plates (Fig. 2(b)). This additional detailing was adopted to delay beam local buckling for drifts equal or higher than those expected under the maximum considered earthquake (MCE) (Eurocode 8).

Fig. 3 shows the experimental hysteresis from the large-scale connection tests. The experimental results showed that the proposed PT connection has robust self-centering behavior by eliminating residual drifts and beam damage for drifts lower or equal to 6%. In addition, repeatable tests on a connection specimen were conducted along with replacing damaged WHPs. These repeatable tests showed that WHPs can be easily replaced without welding or bolting and verified that the proposed connection can be easily repaired with minimum disturbance to building use or occupation in the aftermath of a major earthquake.

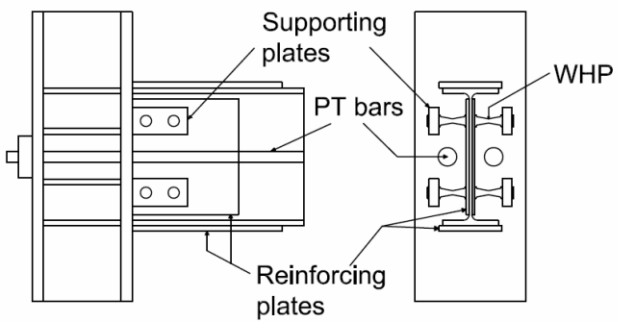

a)

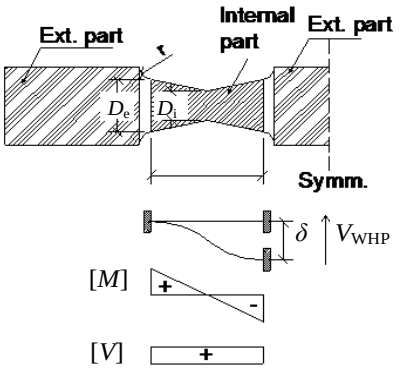

b)

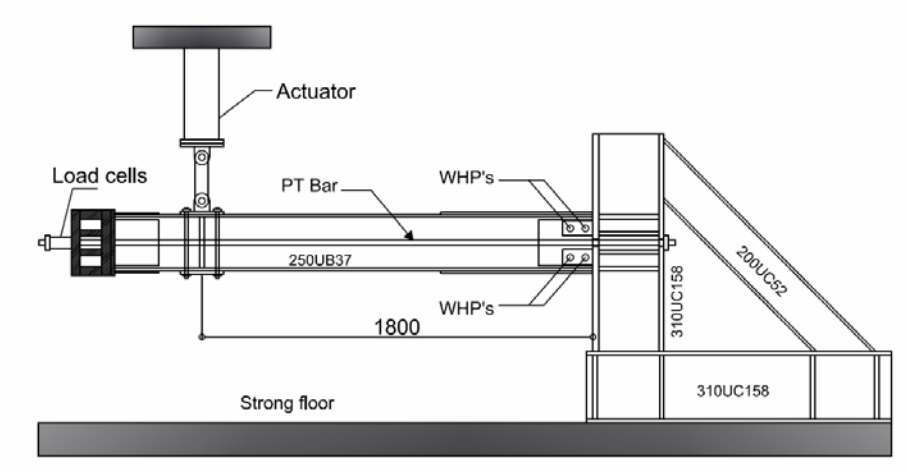

c)

Figure 1. PT connection with WHPs recently proposed and tested by the authors: a) details of the connection region; b) shape and assumed static system of the WHPs; and c) test setup.

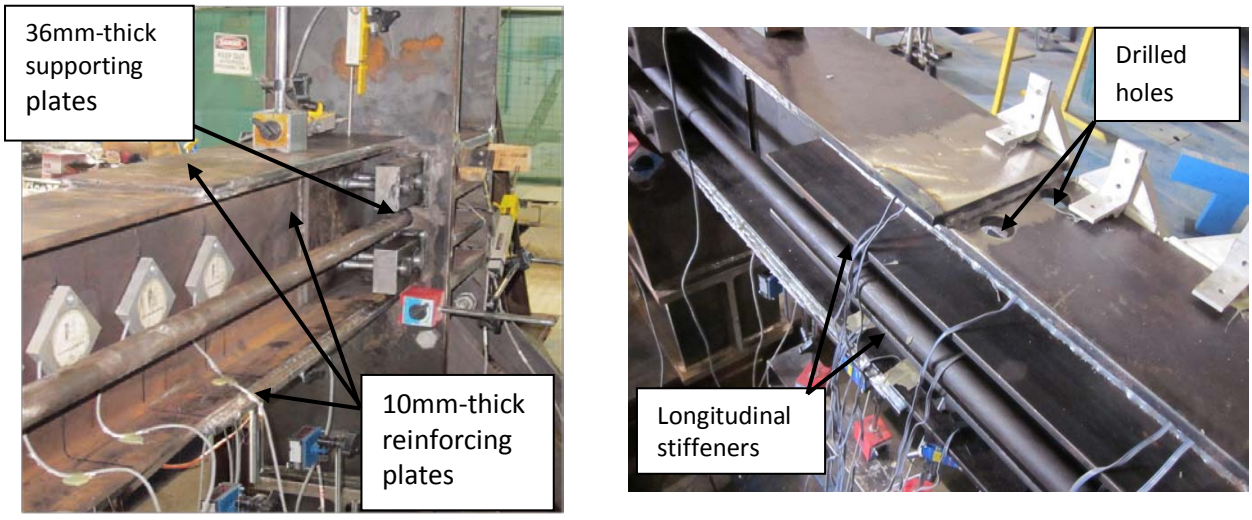

a) b)

Figure 2. Details of the specimens tested in [15]: a) SC-WHP1; and b) SC-WHP2.

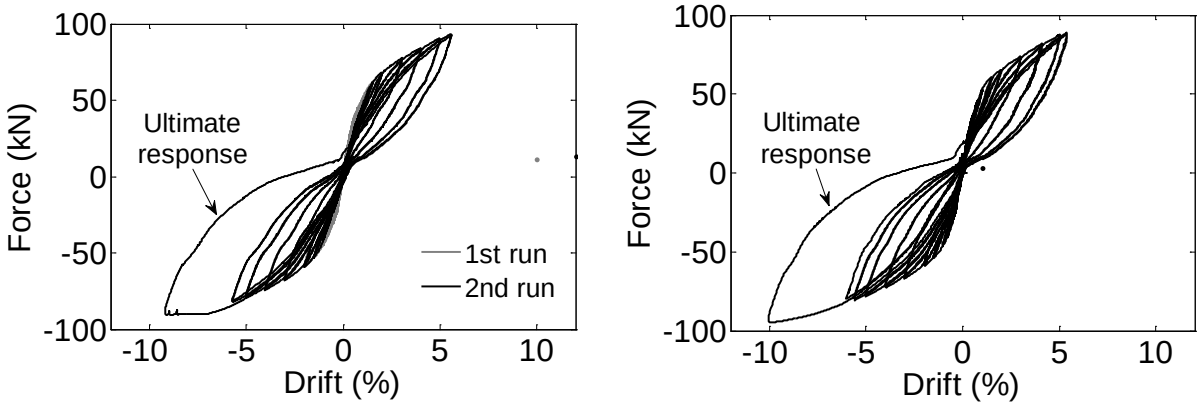

a) b)

Figure 3. Experimental hysteresis of the connections tested in [15]: a) specimen SC-WHP1; and b) specimen SC-WHP2.

3. NONLINEAR FINITE ELEMENT MODELS

3.1 Models for the WHPs

To simulate the cyclic behavior of the WHPs, a three-dimensional FEM model was developed using the commercial software ABAQUS (Abaqus user's manual, 2010). The FEM model geometry reproduced the actual geometry of the test setup of the component tests that were carried out by the authors (Vasdravellis et al., 2012) to characterize the behavior of the WHPs.

Fig. 4 shows the setup used for the WHPs characterization tests along with the FEM model and its boundary conditions. Since the actual geometry was symmetric, only one-fourth of the specimens was modeled to decrease computational time. Both WHPs and supporting plates were modeled using the C3D8R linear hexahedral solid element with reduced integration available in ABAQUS. An elasto-plastic material law with isotropic hardening rule was specified for the supporting steel plates according to the nominal values of the steel properties provided by the manufacturer, while the actual steel material properties from the coupon tests in Vasdravellis et al. (2012) were specified for the WHPs. The WHPs were made of 1020-Grade carbon steel with average yield strength 557MPa, ultimate strength 598MPa, and elongation at fracture equal to 20%. The nominal stress σ_{nom} - nominal strain ε_{nom} curves were converted into piecewise linear true (or Cauchy) stress σ_{true} - logarithmic plastic strain $\varepsilon_{\text{ln}}^{\text{pl}}$ curves, as required for the input in the material properties module according to the relationships:

$$\sigma_{\text{true}} = \sigma_{\text{nom}}(1 + \varepsilon_{\text{nom}}) \tag{1}$$

$$\varepsilon_{\text{ln}}^{\text{pl}} = \ln(1 + \varepsilon_{\text{nom}}) - \frac{\sigma_{\text{true}}}{E} \tag{2}$$

Contact interactions were applied between the cylindrical external surface of the WHP and the holes of the supporting plates. The surface-to-surface contact formulation technique with small sliding between the contacting surfaces was chosen. The contact definition includes the specification of two surfaces, one acting as the "master" surface and the other as the "slave" surface. The contact algorithm searches whether the nodes of the slave surface are in contact with the nodes of the master surface and enforces contact conditions in an average sense over a region of slave nodes using a Lagrange multiplier formulation.

Several simulations were conducted to identify the mesh refinement required to achieve the desired accuracy. The final mesh discretization used hexahedral finite elements with maximum side length of 6 mm and sixteen elements were specified along the perimeter of the cylindrical surfaces. The imposed displacement history used for the component tests was applied to the FEM model; consisted of half-cycles of increasing amplitude with values starting from 0.75mm up to 14mm applied to the internal supporting plate. Displacement-controlled non-linear analysis was performed along with automatic stabilization as fraction of the total energy dissipated in the model in order to ensure that numerical problems due to the contact interactions will not be encountered.

Fig. 5 shows the deformed shape of the WHP and the equivalent plastic strain (*PEEQ*) distribution at a displacement of 12mm. The *PEEQ* is defined as (Abaqus user's manual, 2010):

$$PEEQ = \sqrt{\frac{2}{3}\varepsilon_{\text{ij}}^{\text{p}}\varepsilon_{\text{ij}}^{\text{p}}} \tag{3}$$

where $\varepsilon_{\text{ij}}^{\text{p}}$ is the plastic strain components in the i and j directions. Fig. 5(a) shows that the hourglass shape geometry results in uniform distribution of plastic deformation along the length of the internal part of the WHP, while the external parts of the WHP and the supporting plates are essentially elastic.

The *PEEQ* distribution in the WHP's supporting plates is plotted separately in Fig. 5(b) which shows minor plastic concentrations. These results agree with the experimental test observations (Vasdravellis et al., 2012) where a negligible ovalization of the holes of the supporting plates was evidenced.

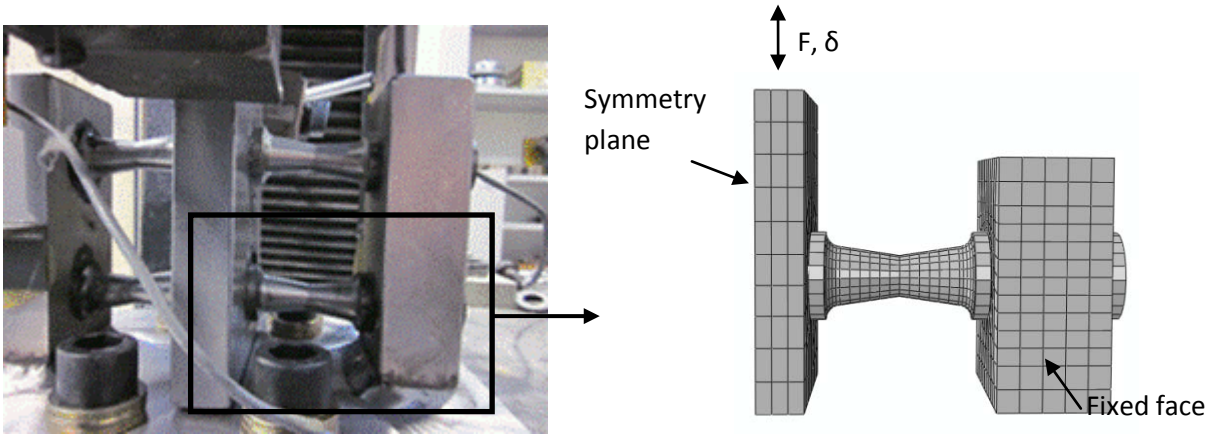

Figure 4. The FEM model used for the WHPs.

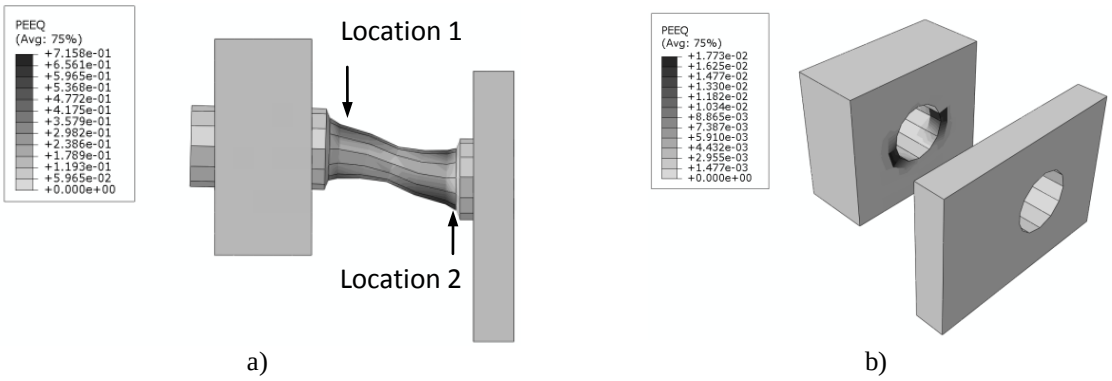

a) b)

Figure 5. Deformed shape of the WHP and equivalent plastic strain (*PEEQ*) contour plot.

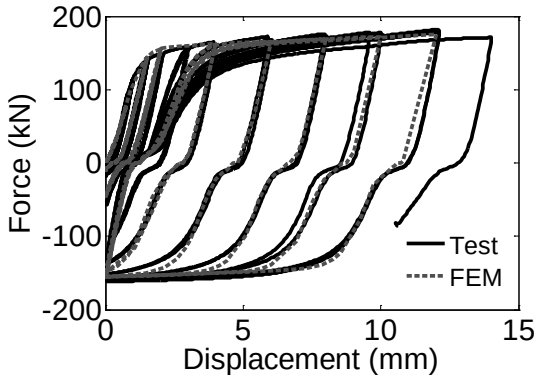

Figure 6. Comparison of the experimental and the numerical force-displacement hysteresis of the WHPs.

Fig. 6 compares the force-displacement hysteresis from FEM analysis with the experimental hysteresis from the WHPs characterization tests. The FEM model can trace the nonlinear cyclic behavior of the WHPs with good accuracy. The model captures the pinching behavior at zero force which is observed in the experimental hysteretic curve as the result of the negligible ovalization of the holes of the supporting plates. Fig. 6 shows that the experimental hysteresis of the WHPs deteriorates after a

displacement amplitude of 12mm. The WHP failed due to ductile fracture at the section close to the internal support plate under a displacement amplitude of 12 mm. The location of the fracture initiation is indicated in Fig. 5(a) as 'Location 2'.

3.2. Models for the connection

A three-dimensional FEM model was developed to simulate the behaviour of the connections as shown in Fig. 7. The commercial software ABAQUS (Abaqus user's manual, 2010) was used for the simulations. The geometry of the tests was reproduced in full detail. The welded interfaces, i.e., the WHP supporting plates welded on the column flange, all the stiffeners welded on the beam and column, and the anchor block attached to the tip of the beam were modelled by applying equal constraints for the degrees of freedom of the nodes at the interface. Contact interactions were specified between surface pairs that separate after contact. The contact surface pairs in the connection are: the bearing interface; the PT bars and the column holes; and, the WHPs and the supporting plates' holes. The column, the PT bars, the WHPs and the plates were modelled using C3D8R solid elements. The beam was modelled using solid elements with incompatible modes (C3D8I). C3D8I are first-order elements that are enhanced by incompatible modes to improve their bending behaviour (Abaqus user's manual, 2010). The mesh was refined in regions where severe plastic deformations or buckling phenomena were expected to occur, i.e., close to the beam-column interface and at the end of the beam flange reinforcing plates. A coarser mesh was used for regions that were expected to remain essentially elastic, i.e., the anchor block, the tip of the beam and the top and bottom parts of the column.

The material properties used in the FEM models are consistent with those used for the initial design of the experimental specimens. For the calibrated FEM models, the stress-strain relationships using nominal material property values were converted into piecewise linear true stress-logarithmic plastic strain curves and used to define the uniaxial material properties of the steel sections, reinforcing plates and PT bars. The uniaxial stress-strain curve for the WHPs was consistent with the material tests described in[Vasdravellis et al. (2012). An elasto-plastic law with isotropic hardening rule was specified for the steel material.

The vertical load was applied as an imposed displacement, U_2, at a distance equal to 1800mm from the connection face as shown in Fig. 7(b). The analysis consisted of several steps. In the first step the contact interactions were established to ensure that numerical problems due to contact formulation will not be encountered during the next steps. The post-tensioning force was applied during the second analysis step by imposing an axial displacement at the free ends of the PT bars capable of producing the desired post-tension force in the beam. In the subsequent steps the cyclic displacement history was applied. Displacement-controlled non-linear analysis was performed along with automatic stabilization as fraction of the total energy dissipated in the model (Abaqus user's manual, 2010) in order to ensure that numerical problems due to the contact interactions will not be encountered. The FEM model consisted of 14574 elements, 25714 nodes, and was solved for a total of 75354 variables. The total computational time of each of the cyclic analyses was 4 hours in a second- generation Intel i7 CPU at 2.80GHz and 8Gb of RAM running in a 64-bit Windows 7 environment.

6.2. Assessment of the FEM models

Fig. 8 plots the force-drift hysteresis from FEM analyses along with the experimental hysteresis of the two connection specimens. The FEM model can capture well the overall cyclic behaviour of the connections. The predicted values are in very good agreement with the corresponding experimental ones, while the initial and post-elastic stiffness are almost identical. The variation of the PT force resulting from the experiments is compared with the FEM prediction in Fig. 9. The FEM simulations and experiments are in relatively good agreement. The numerical model predicts a slightly smaller loss in PT force than that measured in the experiments for specimen SC-WHP1, while the loss in PT force is more accurately predicted for specimen SC-WHP2.

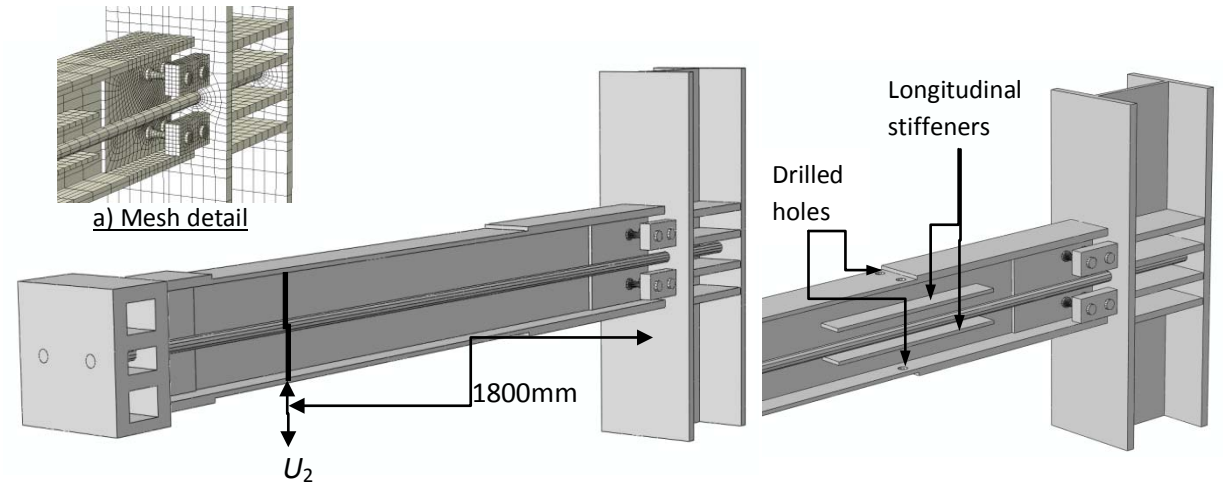

Figure 7. FEM model details: a) FEM discretization; b) model for specimen SC-WHP1; and c) model for specimen SC-WHP2.

Following the loading protocol of the experimental program, the FEM models were pushed to large drifts to investigate all possible global and local failure modes. Fig. 8 shows that the two large last cycles of 9% drift for specimen SC-WHP1 and 10% drift for specimen SC-WHP2 resulted in residual inelastic drifts and loss of self-centering capability. These large drifts resulted in different failure modes of the two connection specimens; consistent with the experimental observations. The FEM model for specimen SC-WHP1 failed due to web buckling immediately after the end of the reinforcing plates. The FEM model for specimen SC-WHP2 failed due to yielding in the region of the drilled holes on the beam flange, and, in the bearing interface, while the web of the beam remained elastic until the end of the analysis. This can be verified by the *PEEQ* values in the deformed configurations of the connections (Fig. 10) for three drift levels: DBE (i.e. Design Basis Earthquake (EC8, 2004) = 1.6%, MCE=2.4%, and Ultimate= 9-10%. In this figure, darker areas indicate larger plastic strain concentration. The FEM models captured the failure modes observed in the experimental program. Fig. 10 shows that under the DBE drift, the connection damage is isolated in the WHPs. Under the MCE drift, damage is concentrated in the WHPs and in the beam flanges in the beam-column interface. Damage in the beam-column interface is more evident in the connection SC-WHP2. Under the ultimate drift, damage in the connection is spread along the beam web immediately after the end of the reinforcing plates and in the beam flanges at the bearing interface. Fig. 10(f) shows that damage in the beam flanges is more evident in the SC-WHP2 model.

The comparisons between the FEM analyses and experiments show that the proposed FEM model is capable of reproducing the inelastic response of the tested PT connections up to the ultimate deformation levels and to capture accurately all possible failure modes. Therefore, it is a reliable tool for the simulation of the hysteretic behaviour of PT steel connections and can be used to conduct further studies to investigate the effect of various parameters.

7. CONCLUSIONS

In this paper, a new self-centering post-tensioned connection was validated both experimentally and numerically. The connection uses post-tensioned high-strength steel bars to provide self-centering capability and carefully designed energy dissipation elements that consist of steel cylindrical pins with hourglass shape (WHPs). WHPs have superior energy dissipation and fracture capacity, and are placed between the upper and the bottom flanges of the beam so that they do not interfere with the composite slab. The connection performance was experimentally validated under quasi-static cyclic loading. The specimens were imposed to drift levels beyond the expected design ones to identify all possible failure

modes. Nonlinear finite element models were constructed to trace the inelastic behavior of the connection up the ultimate failure modes. Based on the experimental and numerical results presented herein, the following conclusions are drawn:

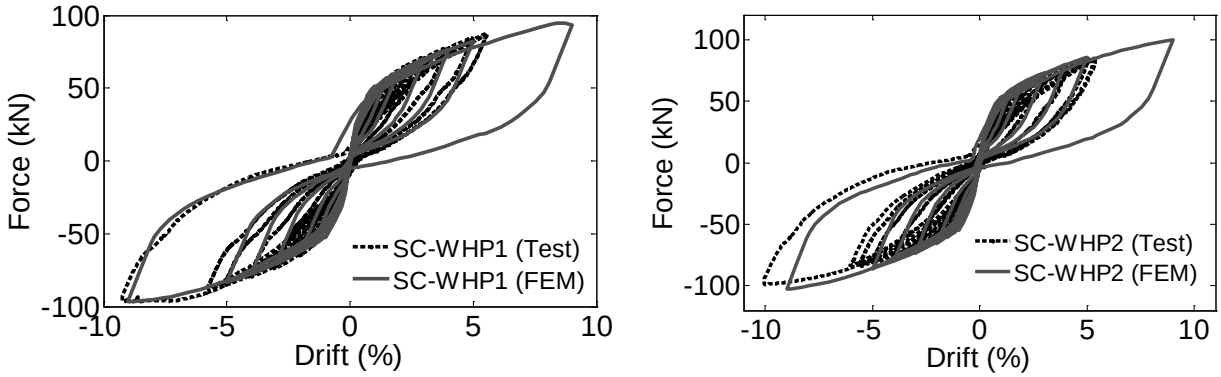

a) SC-WHP1 b) SC-WHP2

Figure 8. Force-drift hysteresis of the two connections specimens tested in [15] and comparison with FEM results: a) SC-WHP1; and b) SC-WHP2

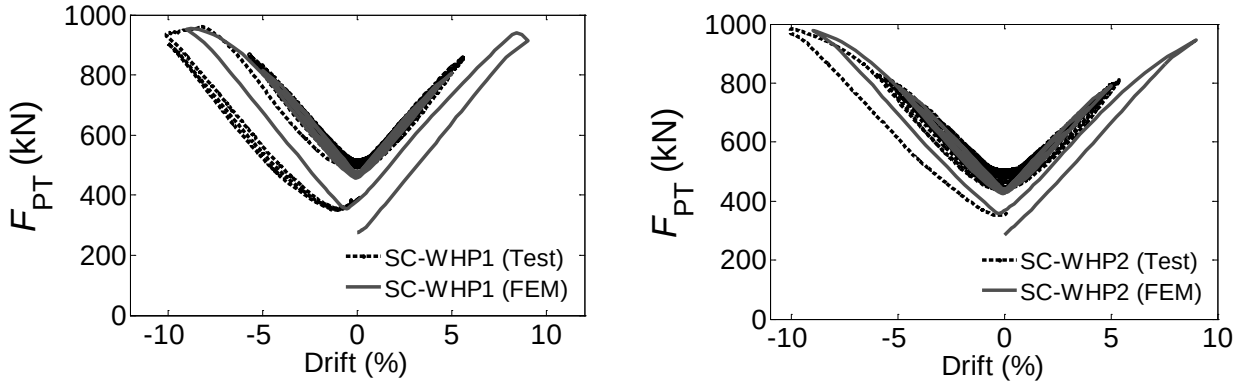

a) SC-WHP1 b) SC-WHP2

Figure 9. F_{PT}-drift plots for the two connection specimens tested in [15] and comparison with FEM results: a) SC-WHP1; and b) SC-WHP2.

- The proposed connection has stable self-centering behavior, enhanced energy dissipation capacity, and, strength and stiffness comparable to those of a welded connection.
- The proposed connection eliminates residual deformations and avoids beam damage for drifts lower or equal to 6%.
- Repeatable tests on a connection specimen were conducted along with replacing damaged WHPs. These tests showed that WHPs can be easily replaced without welding or bolting, and hence, the proposed connection can be repaired with minimal disturbance to building use or occupation in the aftermath of a major earthquake.
- Web local buckling at the connection region after the beam flange reinforcing plates can be avoided by using web stiffeners. However, this detailing results in excessive local yielding at the beam-column interface due to high bearing forces.
- The developed nonlinear FEM models can be reliably used to assess the design of the proposed connection as they are capable to trace the hysteretic behaviour and predict the local failure modes both of the individual WHPs and the connection when subjected to either monotonic or cyclic loading.

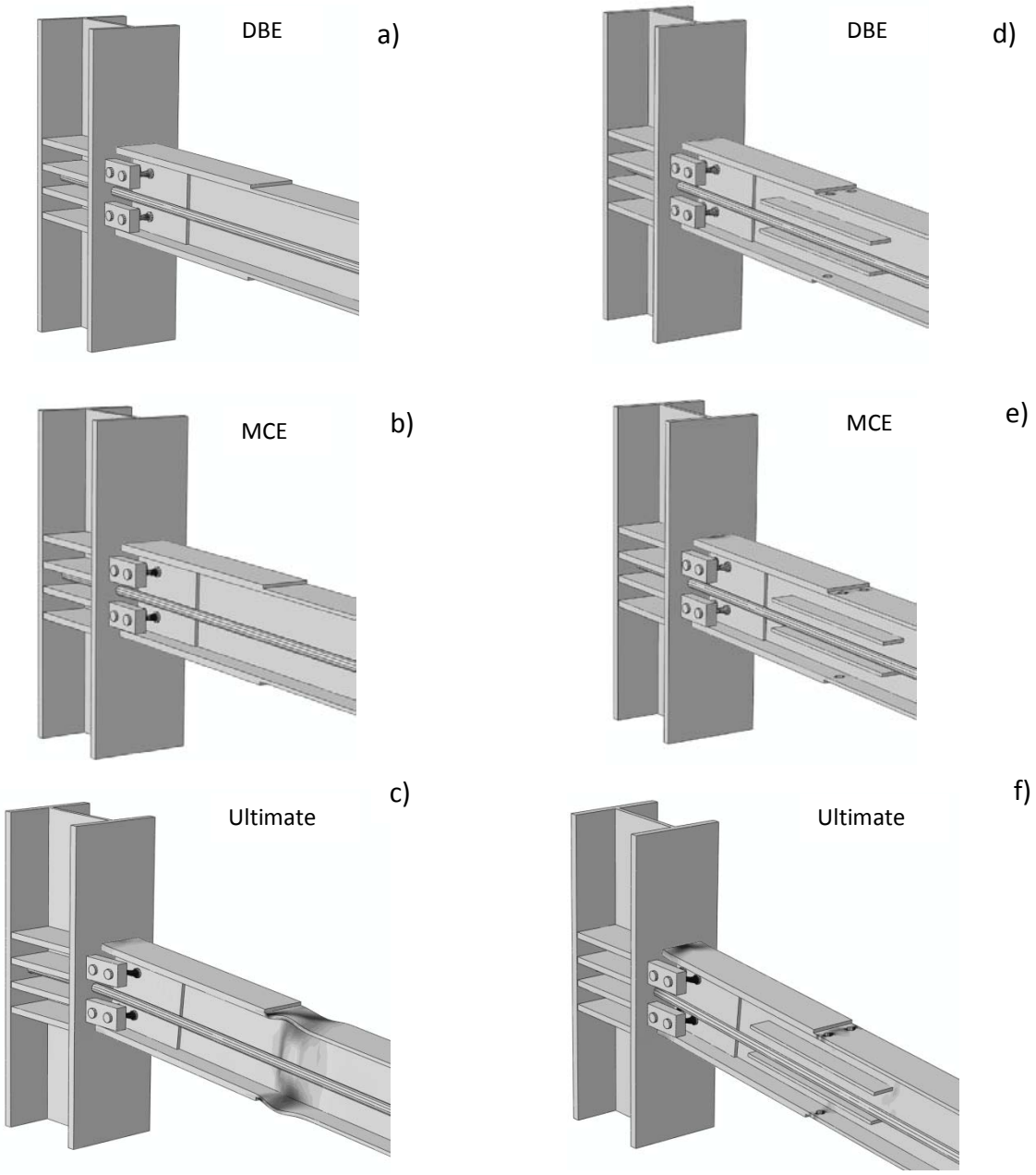

Figure 10. Contour plots of the equivalent plastic strain (*PEEQ*) in the connection at different drift levels: SC-WHP1 (left) and SC-WHP2 (right).

- The FEM analyses confirm that for drifts equal or lower than those expected under the design basis earthquake (DBE), damage in a carefully designed connection is concentrated in the WHPs which are components that can be very easily replaced without welding or bolting.

REFERENCES

Abaqus user's manual, version 6.10 (2010). Dassault Systèmes Simulia Corp., Providence, RI, USA.

AISC (2005). Structural provisions for structural steel buildings. Chicago, Illinois

Christopoulos, C., Filiatrault, A., Uang, C. M., and Folz B. (2002). Posttensioned energy dissipating connections for moment-resisting steel frames. *Journal of Structural Engineering* **128:9**, 1111-1120.

Chou, C. C., Chen, J. H., Chen, Y. C., and Tsai, K. C. (2006). Evaluating performance of post-tensioned steel connections with strands and reduced flange plates. *Earthquake Engineering and Structural Dynamics*

35:9, 1167-1185.
EC8. Eurocode 8 (2004). Design of structures for earthquake resistance
Garlock, M., Ricles, J. M., and Sause, R. (2002). Experimental evaluation of earthquake-resistant posttensioned steel connections. *Journal of Structural Engineering (ASCE)* **128:7**, 850-859.
Garlock, M., Sause, R., and Ricles, J. M. (2007). Behavior and design of posttensioned steel frame systems. *Journal of Structural Engineering (ASCE)* **133:3**, 389-399.
Kim, H. J. and Christopoulos, C. (2009). Numerical models and ductile ultimate deformation response of post-tensioned self-centering moment connections. *Earthquake Engineering and Structural Dynamics* **38:1**, 1-21.
Kobori, T., Miura, Y, Fukuzawa, E., Yamada, T., Arita, T., Takenaka, Y., Miyagawa, N., Tanaka, N., and Fukumoto, T. (1992). Development and application of hysteresis steel dampers. *Earthquake Engineering, Tenth World Conference*: 2341-2346.
Vasdravellis, G., Karavasilis, T.L., Uy, B. (2012). Large scale experimental validation of steel post-tensioned connections with web hourglass pins. *Journal of Structural Engineering* (ASCE). Under Review.